General model and control of an n rotor helicopter

Sidea, Adriana-Gabriela; Brogaard, Rune Yding; Andersen, Nils Axel; Ravn, Ole

Published in:
Journal of Physics: Conference Series (Online)

Link to article, DOI:
10.1088/1742-6596/570/5/052004

Publication date:
2015

Document Version
Publisher's PDF, also known as Version of record

General model and control of an n rotor helicopter

A G Sidea[1,3], R Yding Brogaard[1,2,3], N A Andersen[1] and O Ravn[1]
[1] Department of Electrical Engineering, Technical University of Denmark, Elektrovej 326, 2800 Kongens Lyngby, Denmark
[2] FORCE Technology, Park Allé 345, 2605 Brøndby, Denmark

E-mail: agsidea@elektro.dtu.dk, ryb@force.dk

Abstract. The purpose of this study was to create a dynamic, nonlinear mathematical model of a multirotor that would be valid for different numbers of rotors. Furthermore, a set of Single Input Single Output (SISO) controllers were implemented for attitude control. Both model and controllers were tested experimentally on a quadcopter. Using the combined model and controllers, simple system simulation and control is possible, by replacing the physical values for the individual systems.

1. Introduction

Multi rotor helicopters are a type of unmanned aerial vehicles used for various purposes, ranging from entertainment flights to professional photography and surveillance. Although different designs are available, the most common is the one with an even number of rotors greater or equal to four, uniformly distributed on a circle in the horizontal plane. This is sometimes called “star configuration”.

Multirotors are inherently unstable systems, requiring precise control in order to fly. To implement the required controllers, an accurate system model is needed. Due to system nonlinearity and aerodynamic relations, the system model is complex and different for each configuration.

Various studies related to multirotor modelling and position control were conducted. Starting from the simplest type of multirotors, quadcopters [1], to hexacopters [2] and octocopters [3], multirotors are widely analysed.

Nevertheless, most of the related work implemented models for a fixed number of rotors. In [4], various multirotor configurations are presented, but the modelling still focuses on an octocopter. [5] introduces a modular system that can have varying configurations and number of rotors. However, the modules are autonomous, constituting a cluster of individual rotors working together rather than a single multirotor.

This paper largely presents the results of the master thesis written by Rune Yding Brogaard [6]. The novelty of this work is that it presents a dynamic model that describes the general behaviour of the so-called star configuration. The used equations are derived as a function of number of rotors, denoted with n, which can be replaced with any even number greater or equal to four. This means the model is valid for any multirotor that has the given configuration.

Similarly, equations for flight control were derived to adapt to a variable number of rotors. Attitude control implies controlling each of the roll, pitch and yaw rotations. Having rotation angles as system inputs, the SISO controllers were designed to control the multirotor roll and pitch angles along with

[3] To whom any correspondence should be addressed.

roll, pitch and yaw velocity. With the help of the model, their optimal gains can be found and the multirotor can be given the desired attitude.

2. System equations

When considering multirotor equations, two sets of coordinate axes can be used. The first one, called helicopter-fixed frame (HF), moves together with the helicopter when it rotates, while the second one, called Earth-fixed frame (EF), remains fixed with respect to Earth. In hover, the helicopter fixed frame is the same as the earth frame. These axes can be seen in figure 1, together with the directions of rotation, roll ϕ, pitch θ and yaw ψ.

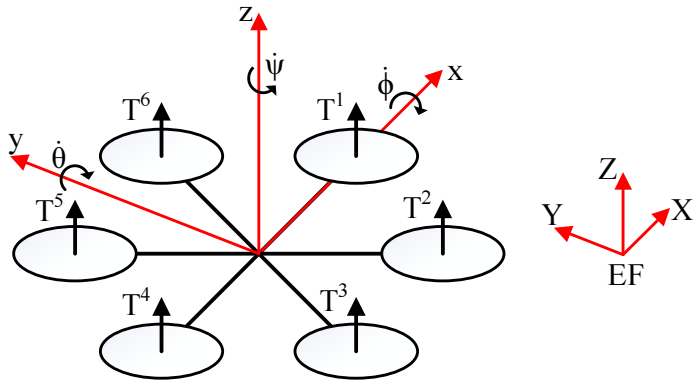

Figure 1. Hexacopter rotation angles in helicopter-fixed frame and Earth-fixed frame.

Before implementing a model for a multi rotor helicopter, formulae for each rotor have to be derived. To show which parameters are different for each rotor, the index i was used in formulae, where i ranges from 1 to n. The index was used as a superscript in order to avoid conflicts with common notations.

According to [7], the formulae for vertical thrust T^i and torque Q^i generated by each rotor have the form shown in (1) and (2). Also, the power required to produce T^i is given in (3).

$$T^i = C_T^i \rho A \left(\Omega^i R_r\right)^2 \tag{1}$$

$$Q^i = C_Q^i \rho A \left(\Omega^i R_r\right)^2 R_r \tag{2}$$

$$P^i = C_P^i \rho A \left(\Omega^i R_r\right)^3 \tag{3}$$

In the previous equations, ρ is the air density, A is the rotor disc area, Ω^i the rotor angular velocity and R_r the rotor radius. The formulae for thrust constant C_T^i, torque constant C_Q^i and power coefficient C_P^i from (4), (5) and (6) are given in [7] as well.

$$C_T^i = \frac{a\sigma}{4}\left(\theta_t - \frac{\dot{z}^i + v_i^i}{\Omega^i R_r}\right) \tag{4}$$

$$C_Q^i = \frac{C_d}{8} + \frac{C_T^i}{\sigma}\frac{\dot{z}^i + v_i^i}{\Omega^i R_r} \tag{5}$$

$$C_P^i = k C_T^{i\frac{3}{2}} + \frac{\sigma C_d}{8} \tag{6}$$

Here, a is the lift slope of the blade, θ_t is propeller angle at the tip, $\dot{z}^i$ is the rotor velocity in z direction of HF (see figure 1), and C_d is the drag coefficient. Although the drag coefficient depends on factors such as Reynolds number or Mach number, it does not change in the used working range [7], hence it does not have an index. k is the induced power correction factor, which takes tip losses, wake swirl and non-uniform inflow into account. Solidity ratio σ is defined by the propeller blade area divided by rotor disc area.

Induced velocity, v_i^i, represents the velocity of air passing through each propeller area in hover. It can be found by using (7).

$$v_i^i = \left(\frac{T_h^i}{2\rho A}\right)^{\frac{1}{2}} \tag{7}$$

Hover thrust can be replaced with the formula in (8), where m is total helicopter mass and g is the gravitational acceleration.

$$T_h^i = \frac{mg}{n} \tag{8}$$

Equation (1) yields the formula for angular velocity:

$$\Omega^i = \frac{\sqrt{C_T \rho A T^i}}{C_T \rho A R_r} \tag{9}$$

By dividing (2) and (3), a relation between power and torque can be derived:

$$\frac{Q^i \Omega^i}{C_Q^i} = \frac{P^i}{C_P^i} \tag{10}$$

Since by definition $P = Q\Omega$, it results that $C_Q^i = C_P^i$. Taking this into consideration, from (9) and (3) the individual power for each rotor is:

$$P^i = \frac{C_Q^i T^i \sqrt{C_T^i \rho A T^i}}{{C_T^i}^2 \rho A} \tag{11}$$

After replacing thrust from (11) with the formula from (8), the power required for hovering is obtained:

$$P^i = \left(\frac{m^3 g^3 {C_Q^i}^2}{{C_T^i}^3 \rho A n^3}\right)^{\frac{1}{2}} \tag{12}$$

By dividing (2) by (1), the ratio between torque and thrust is obtained. It was shown in [6] that there is a linear relationship between the two, thus another coefficient can be introduced as follows:

$$C_{QT} = \frac{Q^i}{T^i} = \frac{C_Q^i R_r}{C_T^i} \tag{13}$$

3. Multirotor model

As mentioned previously, n has to be an even number and the rotors evenly distributed on the *xy* plane. In this case, the angle between each rod is $2\pi/n$, with the rod length from centre to rotor shaft $l \geq R_r/sin(\pi/n)$.

Due to system complexity, some assumptions need to be made to simplify the modelling process:

- The rotors are counted clockwise, with the first one being located on the *x* axis. They alternate between clockwise and counter-clockwise rotation.
- The multirotor centre of mass coincides with the origin of HF, which is situated at the intersection of rods.
- The structure is rigid, including the rotors (no blade flapping or coning).
- Propellers have an ideal blade twist.
- Thrust and torque are considered proportional, their ratio denoted with C_{QT}^{i}.

Figure 2 displays a block diagram of the system, where the control signals for rotation angles (U_ϕ, U_θ, U_ψ) and vertical thrust (U_T) are system inputs. To obtain the desired position, the correct input has to be given to each rotor. The rotors influence the roll, pitch, yaw rotations differently, depending on their geometrical positioning. Considering that they are distributed uniformly on a circle, the angles between them and the axes depend on the number of rotors. Thus, a general formula can be derived that describes each rotor's influence on the three rotations. This can be seen in (14), where *i* denotes the rotor number. The distributor converts the given input signals to the required rotor inputs, which are contained in vector *u*.

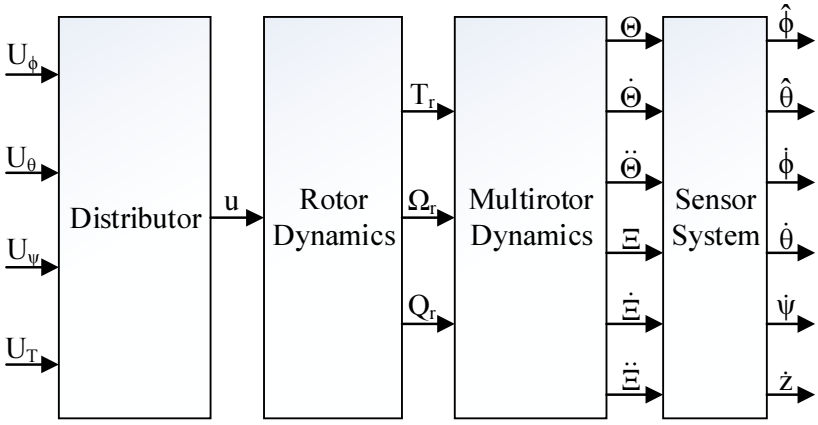

Figure 2. Block diagram of multirotor system.

$$u^i = U_T + U_\theta \, cos\frac{2\pi(i-1)}{n} + U_\phi \, sin\frac{2\pi(i-1)}{n} + (-1)^i U_\psi \tag{14}$$

For modelling the rotor, the first order transfer function in (15) is considered. Although a simplified version of the real function, it was proven to be accurate enough when comparing with experimental data. Time constant τ depends on motor response time and propeller inertia.

$$M_{tf} = \frac{1}{\tau s + 1} \tag{15}$$

The rotor dynamics block contains the elements in figure 3. C_{pwm} represents the relation between input signal and angular velocity. This differs from system to system, having to be determined through measurements. The C_{pwm} block outputs a vector containing the angular velocities of each rotor, which is used to calculate Ω_r and the vector T_r. The latter contains all thrusts corresponding to each angular velocity. f_T represents the relation from (1). From each thrust value, the corresponding torque is found by multiplying with C_{QT}.

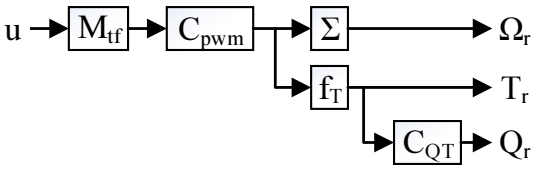

Figure 3. Rotor dynamics.

Ω_r has a single value, calculated as seen in (16). Since the clockwise rotating rotors have odd indexes, they will be subtracted from the sum. This results in a negative or positive value, depending on whether the clockwise or counter-clockwise rotating rotors spin faster.

$$\Omega_r = \sum_{i=1}^{n} (-1)^i \Omega^i \tag{16}$$

Multirotor dynamics can be divided in two types of movement: rotational and linear. To separate them, two vectors are used. $\Theta = [\phi \ \theta \ \psi]^T$ represents helicopter attitude, while $\Xi = [X \ Y \ Z]^T$ represents position in EF. Vectors $\dot{\Theta} = \left[\dot{\phi} \ \dot{\theta} \ \dot{\psi}\right]^T$, $\ddot{\Theta} = \left[\ddot{\phi} \ \ddot{\theta} \ \ddot{\psi}\right]^T$ contain rotational velocities and accelerations respectively. Corresponding vectors for linear movement are constructed using the same principle.

Taking into account the thrust forces, inertial and gyroscopic effects acting on the helicopter, the components for $\ddot{\Theta}$ can be written as:

$$\ddot{\phi} = \frac{\dot{\theta}\dot{\psi}(I_y - I_z) + J_r \dot{\theta} \Omega_r + l \sum_{i=1}^{n} T^i \sin \frac{2\pi(i-1)}{n}}{I_x} \tag{17}$$

$$\ddot{\theta} = \frac{\dot{\phi}\dot{\psi}(I_z - I_x) - J_r \dot{\phi} \Omega_r + l \sum_{i=1}^{n} T^i \cos \frac{2\pi(i-1)}{n}}{I_y} \tag{18}$$

$$\ddot{\psi} = \frac{\dot{\theta}\dot{\phi}(I_x - I_y) + J_r \dot{\Omega}_r + C_{QT} l \sum_{i=1}^{n} (-1)^i T^i}{I_z} \tag{19}$$

These equations were taken from [1] and generalized for n rotors. I_x, I_y, I_z are components of multirotor inertia on each of the axes. J_r is rotor inertia and l is multirotor rod length.
Similarly, position in EF can be found from:

$$\ddot{X} = \sum_{i=1}^{n} T^i \frac{\sin\psi \sin\phi + \cos\psi \sin\theta \cos\phi}{m} \tag{20}$$

$$\ddot{Y} = \sum_{i=1}^{n} T^i \frac{-\cos\psi \sin\phi + \sin\psi \sin\theta \cos\phi}{m} \tag{21}$$

$$\ddot{Z} = \sum_{i=1}^{n} T_i \frac{\cos\psi \cos\phi}{m} - g \tag{22}$$

The sensor system block takes attitude and position vectors, outputting parameters measured by sensors on board the multirotor. Accelerometer and gyroscope measurements are combined to give an

estimation of roll and pitch angles ($\hat{\phi}$, $\hat{\theta}$). The gyro corrects errors resulting from sudden acceleration disturbances, while the accelerometer compensates for drift errors in the gyro [6].

4. Controller model

Because the system inputs are distributed as input signals to each rotor, each rotation around the coordinate axes can be controlled independently. Hence, a set of SISO controllers was implemented for roll, pitch and yaw velocities, as well as for roll and pitch angles. A yaw angle controller was not implemented due to the lack of a heading sensor on the physical system used for testing.

Considering the multirotor does not perform aggressive manoeuvres, it has only small deviations from hovering state. Thus, the system was linearized around this point. In Laplace domain, the linearized angular velocities are:

$$\dot{\phi}(s) = \frac{1}{s}\frac{l\sum_{i=1}^{n} T^i \, sin\frac{2\pi(i-1)}{n}}{I_x} \tag{23}$$

$$\dot{\theta}(s) = \frac{1}{s}\frac{l\sum_{i=1}^{n} T^i \, cos\frac{2\pi(i-1)}{n}}{I_y} \tag{24}$$

$$\dot{\psi}(s) = \frac{1}{s}\frac{J_r\Omega_r s - \Omega_r(0) + C_{QT} l\sum_{i=1}^{n}(-1)^i T^i}{I_z} \tag{25}$$

Both roll and pitch rotations are similar, therefore the controllers implemented for them have the same structure. The only difference between the two is inertia, which depends on the distances between the rotor and the *x* and *y* axes.

Proportional Derivative (PD) controllers were preferred for rotational velocity control due to their higher bandwidth. The steady state error is eliminated by the Proportional Integral Derivative (PID) controllers implemented for the angles.

For the two rotations, the closed loop transfer function of the PD velocity controller is:

$$G^{vel}(s) = \frac{K_P^{vel} LM(s)}{1 + K_P^{vel} LM(s) K_D^{vel}(s) H^{vel}(s)} \tag{26}$$

K_P^{vel} is proportional gain, while K_D^{vel} is the derivative one. *LM* is the linearized model of the system presented in figure 2 without the sensor block. H^{vel} represents the low pass filters of the gyros.

For angle control, G^{vel} was integrated to obtain rotation angle. Having that, the transfer function for angle control could be calculated as:

$$G^{ang}(s) = \frac{K_I^{ang}(s) K_P^{ang} G^{vel}(s)\frac{1}{s} H^{ang}(s)}{1 + K_D^{ang}(s) K_I^{ang}(s) K_P^{ang} G^{vel}(s)\frac{1}{s} H^{ang}(s)} \tag{27}$$

As in the previous case, K_P^{ang} is the proportional gain, K_D^{ang} the derivative one, whereas K_I^{ang} is integral gain. H^{ang} represents the angle estimation system.

Because no controller was implemented for the yaw angle, the steady state error had to be eliminated by using a PID controller for yaw velocity. Its closed loop transfer function is:

$$G^{vel}(s) = \frac{K_I^{vel}(s) K_P^{vel} LM(s) H^{vel}(s)}{1 + K_I^{vel}(s) K_P^{vel} LM(s) H^{vel}(s) K_D^{vel}(s)} \tag{28}$$

5. Model and controller verification

In order to test the designed model and controllers, measurements were performed on a physical system, namely a quadcopter from MikroKopter [8] mounted on a test rig. The specifications for the quadcopter can be found in Table 1. Due to the lack of documentation for some propeller parameters, the thrust and torque constants had to be determined experimentally. By varying rotor speed and measuring thrust and torque each time, relations expressing thrust and torque as a function of angular velocity were found. From these, the constant values were found to be: $C_T = 0.0158\, rad^{-2}$ and $C_Q = 0.023\, rad^{-2}$.

Table 1. Mikrokopter specifications.

Parameter	Value
Propeller radius, R_r	0.126 m
Propeller mass	0.008 kg
Motor mass	0.069 kg
Rod length, l	0.245 m
Rod mass	0.035 kg
Battery mass	0.238 kg
Flight Control Board mass	0.169 kg

The two setups used (figure 4) assured safety and consistency while performing tests. The poles used were high enough to ignore ground effect [9].

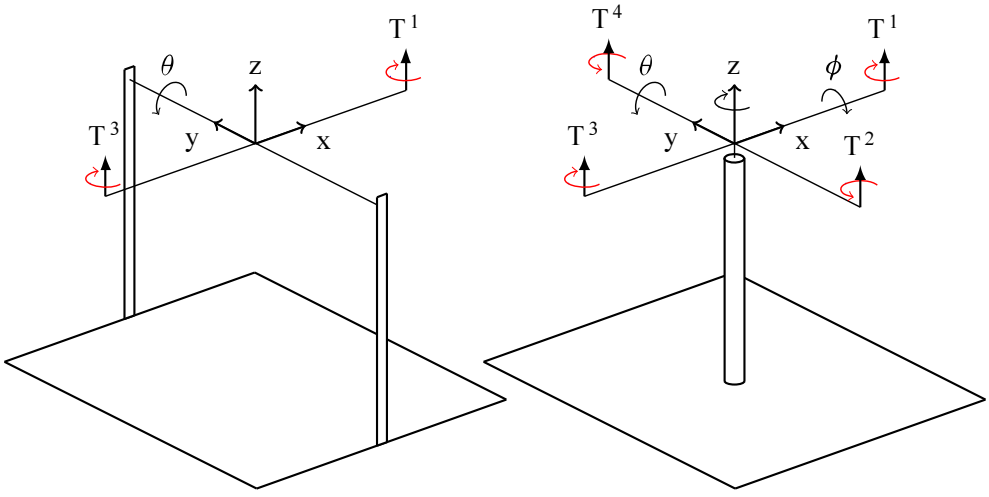

(a) (b)

Figure 4. Experimental setup for testing: (a) roll and pitch rotations, (b) yaw rotation and free rotation along any axis.

Test rig (a) allowed rotation around the *x* or *y* axis by fixing the respective multirotor rods to two vertical poles. Test rig (b) allowed rotation around all axes due to the ball joint mounted at the end of the pole, but it was possible to lock it so that the quadcopter rotated only around *z* axis. Having all the equations derived previously, the quadcopter specifications were introduced in the model. The controller gains were chosen so that the phase margin would be higher than 60 deg. Their discrete transfer functions with sample time 1/487 s can be found in table 2.

In the beginning, each controller was tested separately, by allowing rotation only on one axis. System response was tested by sequentially applying a 0.4 rad/s step input to each angular velocity and 0.4 rad to each angle. After implementing the controllers on the quadcopter, the response to the same step input was measured.

Table 2. Discrete transfer functions of controllers for the tested quadcopter.

Controller	P	I	D
Roll velocity	0.447	–	$\frac{10-9.72z^{-1}}{1-0.72z^{-1}}$
Pitch velocity	0.447	–	$\frac{10-9.72z^{-1}}{1-0.72z^{-1}}$
Yaw velocity	4.467	$\frac{1-0.846z^{-1}}{1-z^{-1}}$	$\frac{10-9.02z^{-1}}{1-0.02z^{-1}}$
Roll angle	2.114	$\frac{1-0.9979z^{-1}}{1-z^{-1}}$	$\frac{10-9.777z^{-1}}{1-0.777z^{-1}}$
Pitch angle	2.114	$\frac{1-0.9979z^{-1}}{1-z^{-1}}$	$\frac{10-9.777z^{-1}}{1-0.777z^{-1}}$

Figure 5 presents the comparison between simulated and measured results for the angle controllers. As it is seen in the figure, simulated response was plotted with a black line, while measured values are represented with a red dotted line. All controllers implemented on the quadcopter are discrete, having a sampling time of 1/487 s.

For testing the PID angle controllers, a step input of 0.4 rad was given. The response has some overshoot due to the integral gain. While the simulation had a 0.196 s rise time and 9.2% overshoot, the real system had lower overshoot of 7.3% at the cost of longer rise time (0.243 s roll and 0.26 s pitch).

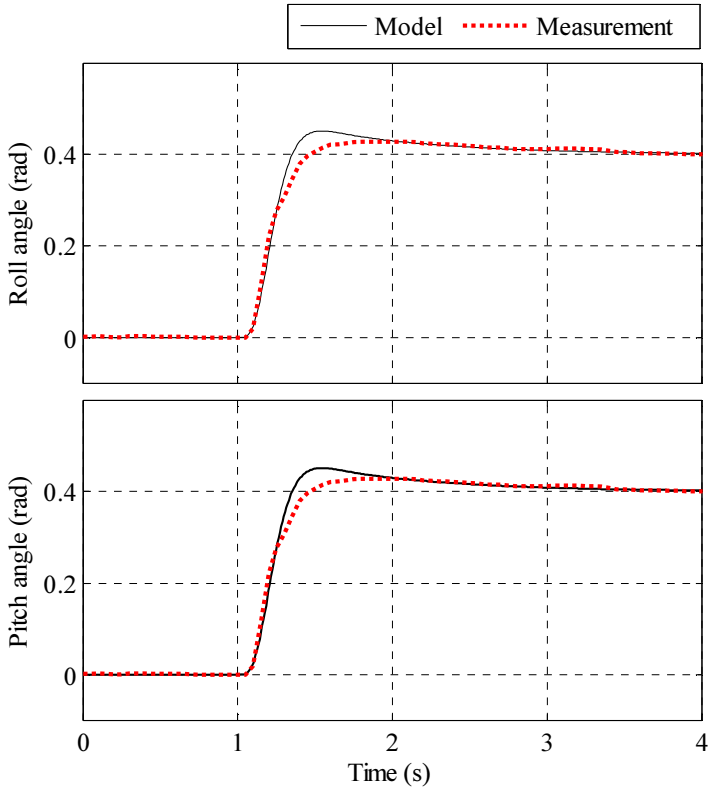

Figure 5. Step response of roll and pitch angle controllers.

The roll and pitch angle responses are very similar, which is no surprise, considering they have the same inertias due to an identical rotor displacement on the x and y axes.

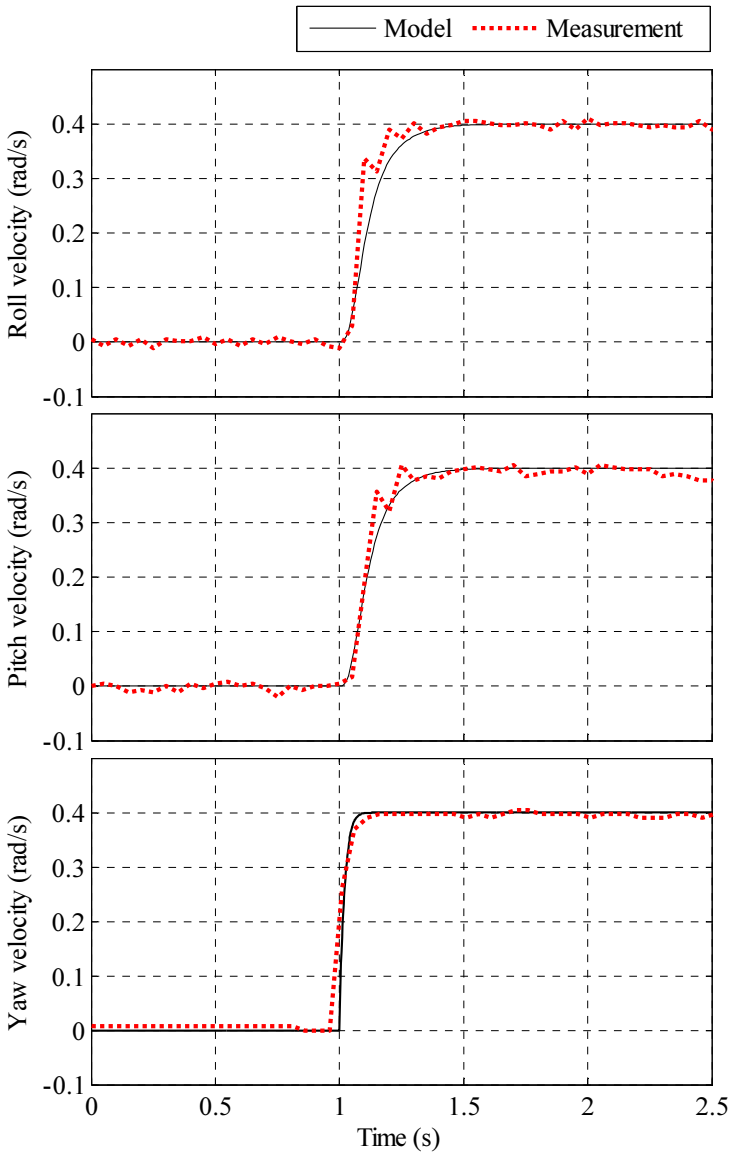

Figure 6. Step response of roll, pitch, yaw velocity controllers.

Figure 6 shows the step responses of the velocity controllers. Measured values follow the simulated ones with only slight deviations. The 0.21 s rise time of the real system for roll and pitch velocities is shorter than the simulated one of 0.26 s.

Yaw velocity has a faster response than the other two, having a simulated rise time of 0.042 s. Again, the measured values are very close to the simulation but the rise time is longer, being 0.056 s.

Although the inaccuracies could have been caused by some uncertainties in the model, the friction forces introduced by the test rigs also had a significant influence.

The previous results show individual responses of all controllers. A flying multirotor however is not restricted on any axis. For this reason, they had to be tested together, to see the influences they have on each other.

Test rig (b) was used for this purpose. This time, the quadcopter could rotate freely on all axes, apart from the 0.5 rad angle limitation caused by the ball joint design. Another thing to be mentioned is that the centre of rotation of the ball joint was at 8 cm distance from the quadcopter's actual one.

A series of step inputs was given to the quadcopter at different times to test controller interactions. The responses of the roll and pitch angle controllers, as well as the one of yaw velocity controller can be seen in figure 7. Simulated results are plotted with continuous lines, while measured ones are represented with dotted lines.

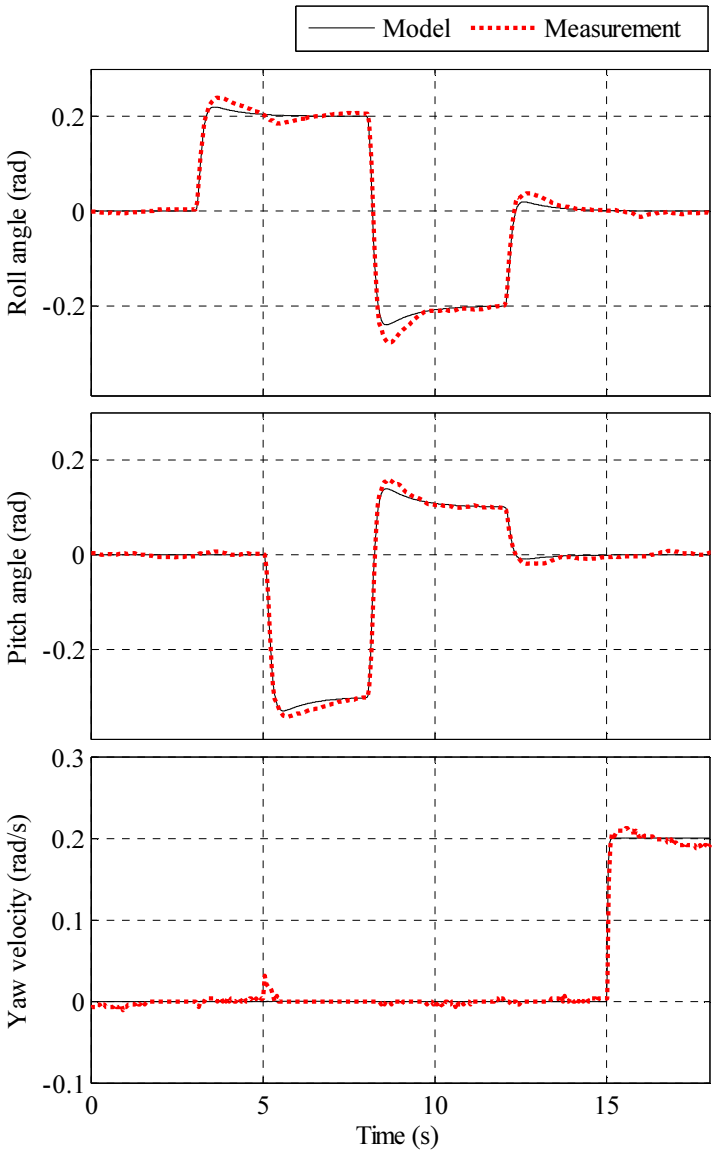

Figure 7. System response to multiple step inputs.

Before the measurement, all angles were set to 0. Step inputs in HF were given as follows:

- At 3 s, a 0.2 rad step was given to the roll angle. The real system had a higher overshoot than the simulated one. No notable influence towards the other rotations could be seen.
- At 5 s, pitch angle received a step of -0.3 rad. A slight decrease of the measured pitch and increase of the measured yaw velocity took place, but they quickly returned to their intended values.

- At 8 s, two steps were given: -0.4 rad for roll and 0.4 for pitch. These set the roll value to 0.1 and pitch value to -0.2 rad. Again, higher overshoot for the real system could be seen, but no changes in the yaw velocity.
- At 12 s, roll received 0.2 rad and pitch received -0.1 rad, returning both angles to 0.
- At 15 s, yaw velocity was given a step of 0.2 rad/s. The roll and pitch angles were not influenced by this change.

The controllers behaved nicely even for inputs very different from the ones required for stationary state. Their influence on each other was minimal, even when two steps were given at the same time. The higher overshoots of the real system were assumed to be caused mainly by the previously mentioned displacement of the centre of rotation.

6. Conclusions

The outcome of this work is a system model independent of the number of rotors that can be used for the configurations where the rotors are uniformly distributed on a circle. Each required parameter can be found by replacing the number of rotors, inertias, etc. in the formulae.

General equations for individual rotors were found and used in the model. Taking into account multirotor geometry and dynamics, the system was described, its equations written as a function of the number of rotors, n.

The designed attitude controllers are also independent of the number of rotors. After specifying the number of rotors and the other required values in the model, the optimal gains can be found for the controllers.

Due to the distributor, SISO controllers could be implemented for each rotation direction. PID controllers were used for roll and pitch angles. In the case of angular velocities, PD controllers were used for roll and pitch because of their higher bandwidth. Yaw velocity required a PID controller to eliminate the steady state error.

An experimental setup was used to see if the designed model and controllers apply to a quadcopter. The fact that the measured values closely follow the simulated ones proves that the model properly recreates the quadcopter physical system.

System simulations showed that the controllers offer a fast and stable response. Not only they perform well individually, but they do this even when combined, having negligible interference on each other.

The model has to be tested on other configurations, but it is expected to give similar results as the four rotor case, provided the correct values for inertias and other system parameters are used.

7. References

[1] Bouabdallah S and Siegwart R 2007 "Full control of a quadrotor" *Int. Conf. on Intelligent Robots and Systems* (San Diego, USA) pp 153-8

[2] Baránek R and Šolc F 2012 "Modelling and control of a hexa-copter" *13th Int. Carpathian Control Conf.* (High Tatras, Slovakia) pp 19-23

[3] Samano A, Castro R, Lozano R and Salazar S 2012 "Modeling and Stabilization of a Multi-Rotor Helicopter" *J. Intelligent and Robotic Systems* **69** 161-9

[4] Rinaldi F, Gargioli A and Quagliotti F 2013 "Proportional Integral Derivative and Linear Quadratic Regulation of a multirotor attitude: mathematical modelling, simulations and experimental results" *Int. Conf. on Unmanned Aircraft Systems* (Atlanta, USA) pp 433-42

[5] Oung R, Ramezani A and D'Andrea R 2009 "Feasibility of a Distributed Flight Array" *Joint 48th IEEE Conf. on Decision and Control and 28th Chinese Control Conf.* (Shanghai, China) pp 3038-44

[6] Brogaard R Y 2012 *Control of Multi Rotor Helicopter* MSc Thesis (Kongens Lyngby,

Denmark: Department of Electrical Engineering, Technical University of Denmark)

[7] Leishman J G 2006 *Principles of Helicopter Aerodynamics* (New York, USA: Cambridge University Press) 2nd ed.

[8] MikroKopter home page, http://www.mikrokopter.de/en/home

[9] Hayden J S 1976 "Effect of the Ground on Helicopter Hovering Power Required" *American Helicopter Society 32nd Annual National V/STOL Forum Proc.*